chrum and other taxa from the Soom Shale of South Africa (*19*). Kaolinite has been reported within the shells of Carboniferous lingulid brachiopods, where it contrasts with the illitic/smectitic composition of the adjacent matrix; the degradation of acidic glycosaminoglycans generated intraskeletal voids and mediated precipitation of clay minerals within them (*20*). Bacteria and other microorganisms can bind metals at their surface that, in turn, act as the nucleation sites for the growth of authigenic minerals, including Fe- and Al-rich silicates (*21*, *22*). The anionic cell surfaces of bacteria that form biofilms may enhance the fossilization potential of decaying leaves by binding cations such as Fe^{3+} (*23*). Detrital minerals can also be adsorbed on the surface of bacterial cells (*21*). Fossilized bacteria have not been identified in association with Burgess Shale fossils, but this does not eliminate a role for microorganisms in the preservation process. They may not have been preserved, or they may have been obliterated during later diagenesis (*15*).

The organic-walled structures recovered from the Burgess Shale include the sclerites of *Wiwaxia* (*6*), the setae of *Canadia* (*6*), and the "thick-walled" [p. 111 in (*7*)] cuticle of *Ottoia* and gut of *Eldonia*. There is no doubt that decay resistance played an important role in the fossilization of these structures. However, the evidence presented here shows that replication by minerals accounts for the detailed preservation of the more labile tissues that makes the Burgess Shale fossils so remarkable.

References and Notes

1. E. H. Davidson, K. J. Peterson, R. A. Cameron, *Science* **270**, 1319 (1995); G. A. Wray, J. S. Levinton, L. H. Shapiro, *ibid.* **274**, 568 (1996); R. A. Fortey, D. E. G. Briggs, M. A. Wills, *Biol. J. Linn. Soc.* **57**, 13 (1996); J. W. Valentine, D. H. Erwin, D. Jablonski, *Dev. Biol.* **173**, 373 (1996).
2. D. E. G. Briggs, D. H. Erwin, F. J. Collier, *The Fossils of the Burgess Shale* (Smithsonian Institution Press, Washington, DC, 1994); S. Conway Morris, *The Crucible of Creation—The Burgess Shale and the Rise of Animals* (Oxford Univ. Press, Oxford, 1998).
3. X. G. Hou, L. Ramsköld, J. Bergström, *Zool. Scr.* **20**, 295 (1991); X. G. Hou and J. Bergström, *Fossils Strata* **45** (116 pp.) (1997); G. E. Budd, *Nature* **364**, 709 (1993); S. Conway Morris and J. S. Peel, *Philos. Trans. R. Soc. London B* **347**, 305 (1995); D. E. G. Briggs and C. Nedin, *J. Paleontol.* **71**, 22 (1997).
4. S. Conway Morris, *Palaeontology* **29**, 423 (1986).
5. H. B. Whittington, *Proc. N. Am. Paleontol. Conv.* **I**, 1170 (1971).
6. N. J. Butterfield, *Paleobiology* **16**, 272 (1990).
7. ———, *Lethaia* **29**, 109 (1996).
8. S. Conway Morris, *Spec. Pap. Palaeontol.* **20** (155 pp.) (1977).
9. K. M. Towe, *Lethaia* **29**, 107 (1996).
10. Analyses were performed on a JEOL JXA8600 Superprobe at an operating voltage of 15 kV (except for the analysis of C, which was performed at 5 kV) with a 32-ms dwell time and a beam current of 15 nA. All elements were scanned in energy-dispersive mode (Oxford Instruments, Buckinghamshire, England, AN10000), except C, which was scanned in wavelength-dispersive mode. Analyses were performed on specimens on the surfaces of planes of splitting and without carbon coating. Potential sources of error in the analysis of uncoated and unpolished samples are due to the effects of surface charging and topography, respectively. In our analyses, the effects of surface charging are minimal: Experimental analyses of the same specimen uncoated and carbon-coated gave similar results except for a slightly sharper image with the latter (see supplementary figure at www.sciencemag.org/feature/data/981648.shl). Topographic effects (most obvious in the preparation marks in the matrix adjacent to the right-hand side of the specimen) are expressed identically for all the elements analyzed (shorter arrow in supplemental figure). However, the relative abundance of elements varies within any anatomical or taphonomic feature, for example, the dark stain associated with *Marrella* (*5*) (longer arrow in supplemental figure).
11. C. D. Walcott, *Smithson. Misc. Collect.* **57**, 145 (1912); *ibid.* **85**, 1 (1931); H. B. Whittington, *Bull. Geol. Surv. Can.* **209** (83 pp.) (1971).
12. Experiments have confirmed that muscle shrinks during early decay [D. E. G. Briggs and A. J. Kear, *Lethaia* **26**, 275 (1993)].
13. Scanning electron microscopy (Cambridge S250 Stereoscan; accelerating voltage of 15 kV) of uncoated samples demonstrated the characteristic texture of sheet silicates. An elemental composition (energy-dispersive x-ray analysis) of Al, K, and Si in variable proportions (Al $\approx$ Si or Al $\ll$ Si) confirmed a dominantly illitic or micaceous composition (*15*).
14. I. Harding [personal communication cited in (*7*)] estimated a temperature of 250° to 280°C for the thermal alteration of the Burgess Shale.
15. S. Conway Morris, in *Palaeobiology: A Synthesis*, D. E. G. Briggs and P. R. Crowther, Eds. (Blackwell, Oxford, 1990), pp. 270–274.
16. Shrimps and prawns collapse as a result of decay, even in the absence of sediment load [D. E. G. Briggs and A. J. Kear, *Palaios* **9**, 431 (1994)].
17. G. A. Logan, M. J. Collins, G. Eglinton, in *Taphonomy: Releasing the Data Locked in the Fossil Record*, P. A. Allison and D. E. G. Briggs, Eds. (Plenum, New York, 1991), pp. 1–24.
18. M. M. Mortland, *Adv. Agron.* **22**, 75 (1970); I. E. Odom, *Philos. Trans. R. Soc. London A* **311**, 391 (1984); G. Lagaly, *ibid.*, p. 315; K. S. Jackson, I. R. Jonasson, G. B. Skippen, *Earth Sci. Rev.* **14**, 97 (1978).
19. S. E. Gabbott, *Palaeontology* **41**, 631 (1998); S. E. Gabbott, R. J. Aldridge, J. N. Theron, *Nature* **374**, 800 (1995).
20. A. Williams and M. Cusack, *Lethaia* **29**, 349 (1997).
21. K. O. Konhauser, W. S. Fyfe, F. G. Ferris, T. J. Beveridge, *Geology* **21**, 1103 (1993).
22. T. J. Beveridge and W. S. Fyfe, *Can. J. Earth Sci.* **22**, 1893 (1985); F. G. Ferris, W. S. Fyfe, T. J. Beveridge, *Chem. Geol.* **63**, 225 (1987).
23. K. A. Dunn, R. J. C. McLean, G. R. Upchurch Jr., R. L. Folk, *Geology* **25**, 1119 (1997).

24. Specimens were kindly loaned by E. J. Loeffler (University of Bristol), D. Collins and D. M. Rudkin (Royal Ontario Museum, Toronto), and the late P. Williamson (Harvard University). S. Powell (photography) provided invaluable assistance; the paper benefited from discussions with D. Robinson, R. J. Parkes, S. E. Gabbott, and R. M. Hazen.

31 March 1998; accepted 14 July 1998

Variation of Interplate Fault Zone Properties with Depth in the Japan Subduction Zone

Susan L. Bilek* and Thorne Lay

The depth dependence of physical properties along the Japan subduction zone interface was explored using teleseismic recordings of earthquake signals. Broadband body waves were inverted to determine the duration of rupture and source depth for 40 interplate thrust earthquakes located offshore of Honshu between 1989 and 1995. After scaling for differences in seismic moment, there is a systematic decrease in rupture duration with increasing depth along the subducting plate interface. This indicates increases in rupture velocity or stress drop with depth, likely related to variation in rigidity of sediments on the megathrust.

Subduction zone earthquakes exhibit spatial variability in rupture processes, including maximum magnitude, subevent complexity, and recurrence rate. Most studies have emphasized along-strike variations in rupture behavior, seeking explanations in terms of plate roughness, age, or convergence rate (*1*). Some studies have addressed spatial variability with depth, emphasizing thermal controls on the seismogenic interplate contact (*2*). Unusual tsunamigenic events that occur at shallow depth have been found to have anomalously long rupture durations, possibly because they occur in low-rigidity sediments (*3*). It is desirable to determine whether rupture properties vary with depth and to relate these variations to expected processes in the fault zone, such as dehydration and cementation of sediments, offscraping of sediments, increasing pressure and temperature conditions, variations in permeability, or phase transitions.

To probe variations in physical properties that may be manifested in earthquake behavior along the subduction zone interface, we used the duration of seismic energy release during faulting as a proxy for rigidity. Rupture duration is dependent on rupture velocity, which is generally found to scale with shear wave velocity v_s (*4, 5*). Rupture duration also depends on the rupture area and the mode of rupture, so it is necessary to scale results for events with

Institute of Tectonics and Earth Sciences Department, University of California, Santa Cruz, CA 95064, USA.

*To whom correspondence should be addressed. E-mail: sbilek@es.ucsc.edu

different seismic moments.

The Japan trench is an ideal location to study the depth dependence of interface properties. This region experiences abundant seismic activity, with variable rupture processes observed for past earthquakes (*6*) and tsunamigenic shallow events (*7*). Additionally, recent studies (*8*) have demonstrated temporally varying slip rates for earthquakes on this interface. Earthquakes in 1992 and 1994 showed large amounts of "slow" slip, ranging from days to 1 year after the events (*8*).

We found 70 possible interplate thrust events of moment magnitude (M_w) 5.0 to 7.7 that occurred between 1989 and 1995 in the Harvard CMT (Centroid Moment Tensor) catalog (*9*). An initial analysis of the corresponding earthquake duration and depth estimates from the Harvard and NEIC (National Earthquake Information Center) earthquake catalogs revealed large scatter, and we tried to improve estimates of both parameters by detailed waveform analysis. We examined teleseismic vertical component broadband records for all events and selected 40 (Fig. 1) for further analysis because of a high signal-to-noise ratio and the availability of stations with good azimuthal coverage (*10*).

Teleseismic *P*-wave recordings (*11*) were used in simultaneous waveform inversions to determine the source depth and source duration for each event (*12*). Inputs into the inversion included the Harvard CMT focal mechanism, azimuth between earthquake and station, *P*-wave velocity (6.0 km/s) (*13*), source depth, and water depth above the source (estimated from bathymetry data). The source depth was varied for each inversion, producing source time functions for 12 to 25 trial depths (*14*). The optimal source depth was determined by minimizing the misfit between the synthetic seismograms generated in the inversion and the real seismograms. The source duration was then estimated from the source time function at the optimal depth by measuring the width of the first large energy pulse (*15*) (Fig. 2). The raw duration estimates were then corrected for size (*15*). We took into account the ambiguity in determining the absolute minimum in misfit and the uncertainty in selecting the termination of the large energy pulse in estimating our error bars on source duration and depth (*16*).

The plate interface is well defined by the selected events at depths of >30 km, but there is more scatter of the events around the defined interface in the shallowest 30 km. If we allow for a ±5 km apparent spread of the megathrust surface due to lateral variations in dip along the strike of the plate boundary, model errors in the depth estimation, and uncertainty in the depth estimates, we can define those events that are compatible with megathrust events (Fig. 3). The outliers from this interface may be attributable to inaccurate event locations or may include intraplate events on thrust faults in the accretionary wedge or within the subducting plate. No events occur less than 35 km from the trench axis; this finding is consistent with other studies of interplate events in this subduction zone (*17*). All events with anomalously long-scaled source durations, >5 s, occur at depths of <20 km (Fig. 3). Overall, there is a progression to ruptures of shorter duration as depth increases.

There is a general trend of decreasing source duration with depth (Fig. 4A). There may be a linear decrease with depth with large scatter, or possibly a stepwise change at around 20 km with large scatter at shallow depth, or some combination. If we assume uniform rupture areas for all of these moment-scaled durations, we can infer rupture velocity variations with depth, which suggests rigidity variations. Variations in rigidity on the fault plane could have progressive and stepwise depth dependence.

Alternatively, it is possible that the rupture area varies systematically, with all events having equal rupture velocity. In this case, the static stress drop σ_s will vary with depth. We calculated σ_s for these events using a circular crack model (*18*). Assuming that the rupture velocity is proportional to v_s, the relation

$$\sigma_s = 7\pi M_o/16 v_s^3 t^3 \qquad (1)$$

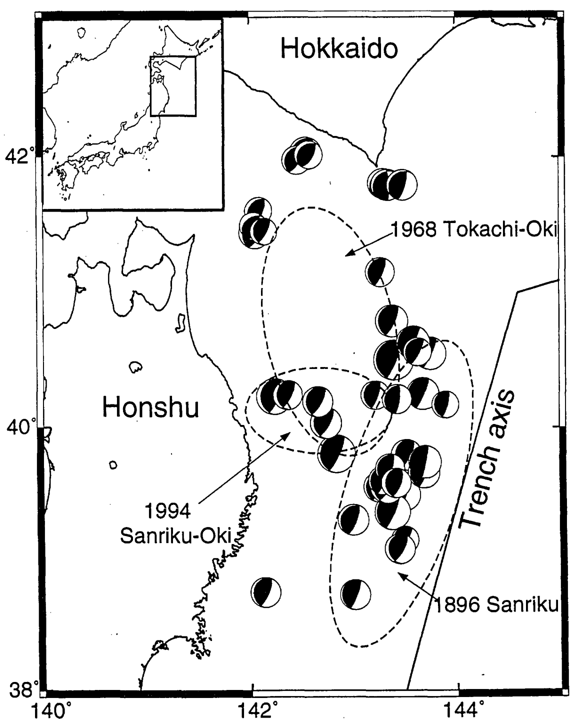

Fig. 1. Source locations from the NEIC catalog, and lower hemisphere focal mechanisms from the Harvard catalog, of the 40 interplate thrust events used in this study. The size of the fault solution reflects the size of the event, with the largest symbol representing an event of M_w = 7.73 and the smallest representing an event of M_w = 5.17. Dashed ellipses show rupture areas of past large earthquakes. Inset gives geographic location of study area.

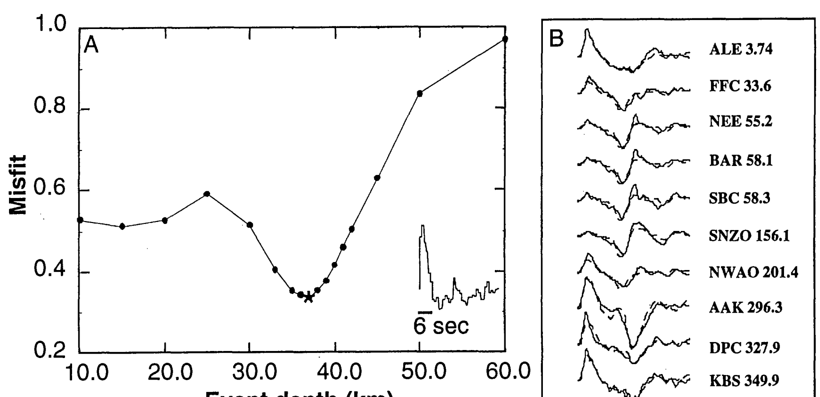

Fig. 2. (**A**) Example of data and inversion results for a M_w 6.95 event on 6 January 1995. Graph shows the residual waveform misfit for each of the 17 point source depths used for this event. The lowest misfit occurs at a depth of 37 km (star), with an error bar of ±1 km. The inset shows the source time function for the estimated centroid depth of 37 km. The source duration for this event was measured to be 6 s. (**B**) The seismograms used for the inversion (data, solid lines; synthetic, dashed lines). Station abbreviations and azimuth from the source are listed.

can be used, where t is the determined source duration, M_o is the seismic moment of the event, and v_s = 3.5 km/s. An increase in estimated stress drop with increasing depth emerges, although there is a large scatter (Fig. 4B). Unfortunately, there is no independent basis for determining the fault area of each event, as is needed to overcome the trade-off between rupture velocity and rupture area (*19*). Also, we lack sufficient resolution to fully characterize the rupture mode of each event.

The relation between source duration and depth (Fig. 4A) suggests variation in physical properties of the subduction zone interface. The rupture process of large earthquakes in this region suggests that there are in fact rupture velocity variations with depth, possibly with a bimodal transition near 20 km depth. The 1896 Sanriku earthquake (Fig. 1) occurred near the trench and had a surface wave magnitude of 7.2 and a tsunami magnitude of 8.2 to 8.6 (*20*). Tsunami records from this event suggest that it had a shallow and slow rupture through low-rigidity subducted sediments (*21*). Two other earthquakes, the 1968 Tokachi-Oki and 1994 Sanriku-Oki events (Fig. 1), had larger seismic magnitudes than the 1896 event but did not produce unexpectedly large tsunamis for their sizes. These two events also had unusual ruptures, with evidence for slow initiation phases along the updip region of the failure zones before the main energy pulses, spanning 20 s for the 1994 event and 30 s for the 1968 event (*22*). For the 1994 event, postseismic "slow" slip was measured for periods up to 1 year, producing a greater moment release than that released in the earthquake itself (*8*). The 1994 event had an average rupture velocity of 1.8 km/s in the shallower portion of the fault (>20 km depth) and 3.0 km/s at greater depth (*23*).

In general, the rigidity of materials increases with increasing depth in the subduction zone, and a relatively abrupt transition in rupture velocity properties with depth—perhaps embedded within this gradual trend—is quite compatible with the data (Fig. 4A). Subducted sediments found along the interface are of lower rigidity than the rest of the subducting plate, and it is expected that events rupturing through these sediments will have anomalously long durations. Sediments along the interface may be responsible for generating shallow tsunami earthquakes, as the fault ruptures into the accretionary wedge or on a sediment-covered megathrust (*3*). In the Japan trench, most sediments are being subducted, as evidenced by the small accretionary wedge (*17*). Multichannel seismic data suggest that these sediments are being subducted to at least 12 km depth, making this a possible zone of weak seismic coupling (*24*).

The presence of fluids on the interface will also influence shear stress and friction at the interface. Friction will be reduced between the two plates when pore pressure is high. Because some water can remain trapped in sediments as they are subducted, pore pressure will be important in determining the frictional properties along the interface. As subduction progresses, water at the interface is usually lost as a result of compaction, thus producing higher rigidity materials (and more frictional resistance) at the interface. The dehydrated, indurated sediments should produce shorter source durations. The effect may be gradual or abrupt, depending on the permeability of the materials in the fault zone.

Water along the interface is also related to phase changes that occur with depth. Low-rigidity smectite retains water and thus provides weakness in the sediment-filled fault zone until transforming to the stronger mineral illite as pressure and temperature increase with increasing depth. This transformation was suggested to influence seismicity with increasing depth (*25*). In the Japan trench, studies have estimated 40 ± 20% smectite in the subducting sediments (*25*).

Plate roughness is another factor that may influence the depth dependence of the interface properties. When the data set is separated into events occurring where the subducting Pacific plate is smooth and events occurring where horst and graben structures are being subducted on the Pacific plate (*6*), we generally see the same trend of long-duration events at shallow depths progressing to the shorter duration events at deeper depths in the smooth regions and only longer duration events shallower than 20 km in the horst and graben regions. The lack of events deeper than 20 km could be due in part to the change in subduction geometry or the smaller event magnitude bounds of our data, but these results suggest that plate roughness does influence these depth-dependent properties.

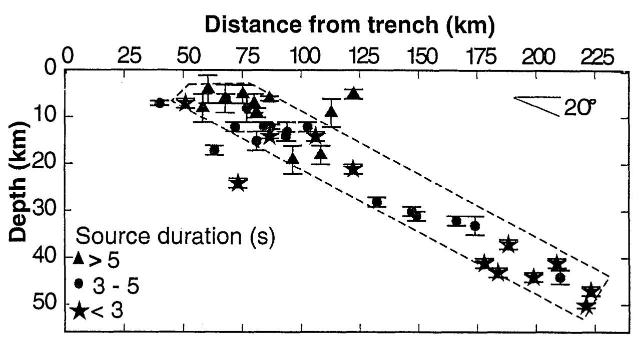

Fig. 3. Normalized source duration and depth of each event as a function of distance (measured from bathymetry data) from the Japan trench. Each source duration is corrected for the moment and normalized to a M_w 6.0 event. Error bars show the depth uncertainty arising from the range in misfit in the inversion. Dashed box encompasses those events that define the plate interface.

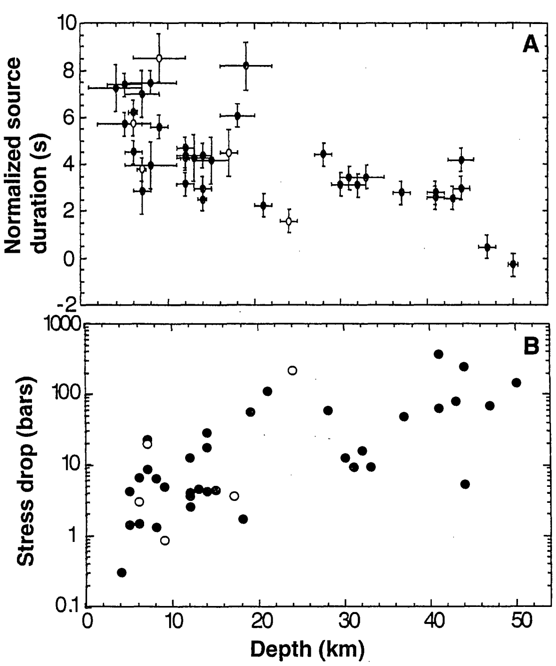

Fig. 4. (**A**) Normalized source duration as a function of depth in the Japan trench. The shallow events have longer rupture durations on average, and rupture duration decreases with depth. Open symbols represent events that do not lie on the plate interface. (**B**) Stress drop as a function of depth in the Japan trench. Stress drop is calculated from the source durations determined from the inversion.

References and Notes

1. L. Ruff and H. Kanamori, *Phys. Earth Planet. Inter.* **23**, 240 (1980); T. Lay, H. Kanamori, L. Ruff, *Earthquake Predict. Res.* **1**, 3 (1982); L. J. Ruff, *Tectonophysics* **211**, 61 (1992).
2. Z. Zhang and S. Y. Schwartz, *J. Geophys. Res.* **91**, 537 (1992); B. W. Tichelaar and L. J. Ruff, *ibid.* **98**, 2017 (1993).

3. Y. Fukao, *ibid.* **84**, 2303 (1979); A. M. Pelayo and D. A. Wiens, *Geophys. Res. Lett.* **17**, 661 (1990); *J. Geophys. Res.* **97**, 15321 (1992); S. Ide, F. Imamura, Y. Yoshida, K. Abe, *Geophys. Res. Lett.* **20**, 863 (1993); H. Kanamori and M. Kikuchi, *Nature* **361**, 714 (1993); K. Satake, *Geophys. Res. Lett.* **21**, 2519 (1994).
4. H. Kanamori and D. L. Anderson, *Bull. Seismol. Soc. Am.* **65**, 1073 (1975).
5. v_s is defined as the square root of the rigidity divided by the density of the material.
6. Y. Tanioka, L. Ruff, K. Satake, *Island Arc* **6**, 261 (1997).
7. Y. Tanioka and K. Satake, *Geophys. Res. Lett.* **23**, 1549 (1996).
8. I. Kawasaki *et al.*, *J. Phys. Earth* **43**, 105 (1995); K. Heki, S. Miyazaki, H. Tsuji, *Nature* **386**, 595 (1997); K. Heki and Y. Tamura, *Geophys. Res. Lett.* **24**, 3285 (1997).
9. The search of the Harvard CMT catalog used the latitude range of 37° to 43° and longitude range of 140° to 145°. The events were classified as interplate if they met the following criteria: The source depths were less than 80 km; the fault plane, taken from the Harvard fault mechanism solution, had a strike within 20° of the strike of the Japan trench axis (195° ± 20°); and the dip of the fault plane was ≤35°. These criteria for interplate thrust event classification are similar to those used in earlier studies (*2*).
10. The chosen events have seismic moments between 7.24×10^{16} N·m and 4.89×10^{20} N·m, and all recordings are from between 30° and 90° from the events. For more data on the 40 events, see *Science* Online (www.sciencemag.org).
11. All seismic records were deconvolved to displacement traces by removing the instrument response. The mean and linear trend were also removed from the data. The onset of the *P*-wave arrival was then manually selected for all seismograms. Between 4 and 12 recordings were used for each event.
12. The inversion is based on deconvolving a point-source Green function from each signal to extract the moment rate history or source time function. A range of source depths is considered, and the simultaneous fitting of azimuthally distributed signals resolves intrinsic trade-offs between source time function and source depth. For a detailed description of the inversion process, see L. Ruff, *Geophys. Res. Lett.* **16**, 1043 (1989); B. Tichelaar and L. Ruff, *J. Geophys. Res.* **96**, 11997 (1991); L. J. Ruff and A. D. Miller, *Pure Appl. Geophys.* **142**, 101 (1994).
13. The *P*-wave velocity of 6.0 km/s is used as the average velocity from the event hypocenter to the free surface. More complex velocity models for the overthrust wedge can be used for the waveform inversion, such as the model of G. Suarez and D. Comte [*J. Geophys. Res.* **98**, 15825 (1993)]. B. Tichelaar and L. J. Ruff (*ibid.*, p. 15829) showed that the depth estimates vary by <4 km between a simple velocity model and the more complex models, with depths of shallower events tending to be slightly overestimated.
14. The first iteration of the inversion used the source depth listed in the NEIC catalog. Trial depths were then chosen in increments of ±5 km, starting around the first iteration depth, and finer increments of 1 km were used to converge on the optimal depth for the event. The depth is measured from the ocean bottom to the hypocenter.
15. Using the Harvard catalog seismic moments for each event, we normalized the measured source durations to a common seismic moment (M_o) using an empirical relationship [correction = 2.25(log M_o) − 50.7] between the centroid time shift and log seismic moment for all shallow thrust events listed in the Harvard CMT catalog. The durations are normalized to an M_w 6.0 event by adding a constant value to each duration. We are confident that the normalization process removes the magnitude effects on duration, as there is no relation between our normalized duration and log M_o for our data set.
16. In some cases there was a range of depths with low misfit. The source duration listed is for the depth with the lowest misfit, and error bars indicate the depth range giving low misfit.
17. K. Suyehiro and A. Nishizawa, *J. Geophys. Res.* **99**, 22331 (1994).
18. The stress drop is related to the fault displacement divided by fault length or width, along with constants dictated by the crack model. Using the definition for the seismic moment of $M_o = \mu AD = \mu\pi r^2 D$ for a circular crack model (where μ is the rigidity, A is the fault rupture area, r is the radius of the circular fault area, and D is the average displacement on the fault), we calculate the stress drop $\sigma_s = 7\pi M_o/16r^3$. Because the rupture velocity $v = r/t$ excess for a circular expanding rupture, the stress drop is inversely proportional to the cube of rupture velocity (taken to be equal to v_s for simplicity) and the cube of source duration used in Eq. 1.
19. J. E. Vidale and H. Houston, *Nature* **365**, 45 (1993).
20. K. Abe, *Phys. Earth Planet. Inter.* **27**, 194 (1981); *Bull. Seismol. Soc. Am.* **84**, 415 (1994).
21. H. Kanamori, *Phys. Earth Planet. Inter.* **6**, 246 (1972).
22. Y. Tanioka, L. J. Ruff, K. Satake, *Geophys. Res. Lett.* **23**, 1465 (1996); S. Y. Schwartz and L. J. Ruff, *J. Geophys. Res.* **90**, 8613 (1985); J. R. Hartog and S. Y. Schwartz, *Geophys. Res. Lett.* **23**, 2037 (1996).
23. W. Nakayama and M. Takeo, *Bull. Seismol. Soc. Am.* **87**, 918 (1997).
24. R. von Huene and R. Culotta, *Tectonophysics* **160**, 75 (1989); R. von Huene, D. Klaeschen, B. Cropp, *J. Geophys. Res.* **99**, 22349 (1994).
25. P. Vrolijk, *Geology* **18**, 703 (1990).
26. We used the program GMT (Generic Mapping Tools) to generate several of the figures. S. Y. Schwartz, R. Hartog, M. Hagerty, and D. Saffer provided helpful comments on the manuscript. This is contribution number 352 of the Institute of Tectonics, University of California, Santa Cruz. Supported by NSF grant EAR-9418643.

1 April 1998; accepted 2 July 1998

Measurements of the Equation of State of Deuterium at the Fluid Insulator–Metal Transition

G. W. Collins, L. B. Da Silva, P. Celliers, D. M. Gold, M. E. Foord, R. J. Wallace, A. Ng, S. V. Weber, K. S. Budil, R. Cauble*

A high-intensity laser was used to shock-compress liquid deuterium to pressures from 22 to 340 gigapascals. In this regime deuterium is predicted to transform from an insulating molecular fluid to an atomic metallic fluid. Shock densities and pressures, determined by radiography, revealed an increase in compressibility near 100 gigapascals indicative of such a transition. Velocity interferometry measurements, obtained by reflecting a laser probe directly off the shock front in flight, demonstrated that deuterium shocked above 55 gigapascals has an electrical conductivity characteristic of a liquid metal and independently confirmed the radiography.

Hydrogen is the simplest and most abundant element in the universe, yet at high pressure, it is one the most difficult to understand. Having only a single electron, it shows characteristics of both the group I alkalis and the group VII halogens (*1*). At low pressure, hydrogen isotopes are halogenous, covalent diatomic molecules that form insulators. With increasing pressure, the isotopes transform into alkali metals. Although most theories predict <300 GPa for the insulator-metal transition pressure along the 0 K isotherm (*2*), static experiments at even higher pressures have not detected evidence of metallization (*3*). Evidence of high electrical conductivity was observed at an unexpectedly low pressure (140 GPa) at finite temperature (3000 K) where the isotope is in a molecular fluid phase (*4*). There is no accepted theoretical description of the transformation of hydrogen from an insulator into a conducting atomic fluid at high pressures and high temperatures.

G. W. Collins, L. B. Da Silva, P. Celliers, D. M. Gold, M. E. Foord, R. J. Wallace, S. V. Weber, K. S. Budil, R. Cauble, Lawrence Livermore National Laboratory, Livermore, CA 94550, USA. A. Ng, University of British Columbia, Vancouver V6T 1Z1, BC, Canada.

*To whom correspondence should be addressed.

The metallic transition and its effects on the equation of state (EOS) at pressures near 100 GPa are integral to models of many hydrogen-bearing astrophysical objects (*5*), including the Jovian planets (*6*), extrasolar giant planets (*7*), brown dwarfs (*8*, *9*), and low-mass stars (*10*), as well as to the design of deuterium-tritium–burning targets for inertial confinement fusion (*11*). The phase space of hydrogen in the vicinity of the finite-temperature insulator-metal transition (Fig. 1) is difficult to address theoretically: it is a dynamic, strongly correlated, partially degenerate composite of H_2, H, H^+, and electrons, as well as other components such as H_3, where no simple approximation is available. This makes reliable experimental data essential as a guide to theory, but meaningful measurements on the Hugoniot (*12*) in this regime have until recently been unattainable. Using a high-power laser, we have accessed this regime by shocking liquid D_2 to pressures at and above the metallic transition where we measured the thermodynamic properties of the shocked state.

At high pressures, molecular dissociation and ionization can be activated through high density as well as thermal effects. Early EOS models either did not include these effects or